Fe-Cr-V 耐磨堆焊合金

龚建勋[1]， 肖逸锋[1]， 张清辉[1]， 马 蓦[2]
（1. 湘潭大学 机械工程学院，湖南 湘潭 411105；2 湘潭大学 物理与光电材料学院，湖南 湘潭 411105）

摘 要：制备了用于埋弧焊药芯焊丝的 Fe-Cr-V 堆焊合金，其成份（质量分数，%）为 C 0.9～1.5，Cr 13～15，V 1.0～2.0. 借助光学显微镜、扫描电镜和 X 射线衍射等手段，研究了其显微组织，并考察 V 和 B_4C 含量对该堆焊合金性能的影响。Fe-Cr-V 堆焊合金的显微组织由铁素体＋马氏体＋$(Cr, Fe)_{23}C_6$ 等碳化物组成。电子能谱微区分析显示 Cr，V 元素晶界含量显著高于晶内，随 WC 加入量提高，晶界与晶内含量差距增大。由于沿晶界析出碳化钒，这使 $(Cr, Fe)_{23}C_6$ 等晶界碳化物呈条状或断续网状分布，起到耐磨骨架作用，避免了网状形态的强烈脆性。结果表明，其磨粒磨损性能显著优于实心焊丝 H25Cr3Mo2MnV 堆焊合金。

关键词：耐磨；堆焊；药芯焊丝；铁素体；碳化物
中图分类号：TG422.1 文献标识码：A 文章编号：0253－360X(2008)07－0073－04

龚建勋

0 序 言

以渣、气或者渣气联合保护方式，在机械零件表面堆焊一层耐磨或者耐腐蚀等金属层，赋予表面以特殊的性能，这项工艺已经为广大企业所采用[1]。所用的焊接材料有药皮焊条、实心焊丝和药芯焊丝，其中药皮焊条电弧堆焊具有操作简单、灵活方便等优点，缺点效率低；实心焊丝刚性强、工艺性能好，但过渡的合金元素量有限；药芯焊丝成分调节极为方便，根据需要可获得所需成分的堆焊合金，埋弧或气保护堆焊方式具有熔敷效率高，更适合于企业生产[2]。国内钢铁企业修复轧辊用实心焊丝 H25Cr3Mo2MnV 的堆焊合金仍存在耐磨性不足的问题，而所研制的药芯焊丝多以 Cr-Mo，Cr-Mo-V，Cr-Ni-Mo-V 合金系为主，如高碳高铬合金，由于形成的网状碳化物过于粗大，韧性差，致使埋弧堆焊时合金易开裂[3]。堆焊合金的耐磨性主要与其显微组织中的硬质相，如碳化物的数量相关，而韧性则取决于基体组织[4]。基于上述分析，作者在大量试验的基础上，选择对 Fe-Cr-V 药芯焊丝堆焊合金的显微组织和耐磨性进行研究。

收稿日期：2007－09－11
基金项目：湖南省教育厅资助项目（06C838）；湘潭大学科研启动基金资助项目（06QDZ05）

1 试验方法

药芯焊丝外皮为 H08A，药芯由高碳铬铁（69% Cr，4%C）、金属铬、钒铁（50%V）、钛铁（30%Ti）、镍粉、铁粉等组成，并向其中添加少量碳化硼（B_4C）、碳化钨（WC）等硬质相粉末。药粉搅拌均匀后经 YHZ-1 药芯焊丝成型机轧制成型，再拉拔减径为 ϕ3.6 mm 焊丝。

在90 mm×70 mm×16 mm的试板（Q235）上，药芯焊丝用交流埋弧焊机 MZ-1000 堆焊三层，工艺参数如表 1 所示，焊剂 HJ260，焊后焊渣自动脱落，焊缝表面光洁，无粘渣。堆焊合金的成分（质量分数，%）为：C 0.9～1.5，Cr 13～15，V 1.0～2.0，Si 0.5～1.5，Mn 0.5～1.2，W 0.4～1.0，Ni 0.8～1.5，B 0.3～1.0，其它余量。

表 1 药芯焊丝埋弧焊工艺参数

Table 1 Processing parameter of flux cored wire submerged arc welding

焊接电流 I/A	电弧电压 U/V	焊丝伸出长度 L/mm	焊接速度 v/(cm·min^{-1})	层温 T/℃	焊后状态
380～420	30～34	30～40	36～42	100～150	空冷

试样表面磨平后，用 HR-150 洛氏硬度计测试硬度，然后线切割加工制备12 mm×12 mm×25 mm金相试样、57 mm×25.5 mm×6 mm耐磨性试样。水冷切取堆焊表层部分，敲碎并研磨为粉末，作为 D/

MAX2550VB 型 X 射线衍射仪分析样品，选取 53～55 号试样进行 XRD 分析，其中 55 号是在 54 号组分的基础上，去除钒铁、B_4C 和 WC 粉末而其它组分保持不变的试样。

金相试样先以 4% 的硝酸酒精，再用复合试剂（硝酸5 ml、盐酸15 ml、重铬酸钾2.5 g、苦味酸1 g、酒精30 ml，以上均为分析纯）依次浸湿。用水和酒精清洗干净后，吹干，在 JSM-6360LV 扫描电镜上观察试样表面，附属电子能谱仪 Oxford 7854 分析其微区成分。

耐磨性试验采用 MLS-23 型湿砂橡胶轮式磨损试验机，条件如下：橡胶轮直径178 mm，邵尔硬度60，所加砝码重2.5 kg，橡胶轮转速240 r/min，砂浆比例为1 500 g石英砂（40～60 目）配1 000 g水。试样先预磨 1 000 r，冲洗干净，吹干，称初重 m_0，然后正式试验1 000 r 后清洗吹干，称重 m_1，（m_0-m_1）即为试样磨损绝对失重量 Δm。以实心焊丝 H25Cr3Mo2MnV（ϕ4.0 mm）堆焊试样作为标准试样 1 号，相对磨损系数 ε＝试样绝对失重量/标准试样绝对失重量，选取 46 号，48 号，49 号，52 号，53 号和 54 号等堆焊合金为试验对象，试样成分区别和试验结果见表 2。试验结束后，将试样表面冲洗吹干，用 JSM-6360LV 扫描电镜观察表面磨损形貌。

表 2 Fe-Cr-V 堆焊合金的耐磨粒磨损性能

Table 2 Abrasion resistance of Fe-Cr-V hardfacing alloy

试样编号	硬度 (HRC)	磨损前 m_0/g	磨损后 m_1/g	绝对失重量 Δm/g	相对磨损系数 ε	药芯中 V, WC, B_4C 的含量（质量分数，%）		
						V	WC	B_4C
1#	43.2	65.293 1	64.242 9	1.050 2	1.00			
46#	59.2	64.480 9	64.377 0	0.103 9	0.099	1.25	1	2.0
48#	58.4	63.916 9	63.902 6	0.014 3	0.014	1.25	2	2.0
49#	62.5	63.668 3	63.649 8	0.018 5	0.017	1.50	1	2.5
52#	58.4	60.420 3	60.387 4	0.032 9	0.031	2.00	1	2.0
53#	59.2	62.210 5	62.188 8	0.021 7	0.021	1.50	1	2.0
54#	60.5	62.388 3	62.369 3	0.014 0	0.013	1.50	2	2.0

2 试验结果及分析

2.1 堆焊 Fe-Cr-V 合金的显微组织

Fe-Cr-V 埋弧堆焊合金的金相组织见图 1。由图1 可知，Fe-Cr-V 合金由基体（铁素体＋马氏体）（灰色＋黑色）和碳化物（白色）组成。与 53 号相比，54 号只是碳化钨加入量多 1 倍，其它组分均相同，但54 号晶界的碳化物分布更为均匀、分散且较小，这表明加入适量的硬质相，可改善晶界碳化物形貌，减少晶界开裂的敏感性。

图2 为 Fe-Cr-V 堆焊合金粉末的 XRD 图谱，由此可知，其基体组织为铁素体＋马氏体，这与金相分析结果一致。55 号的 α-Fe 基体（100）面晶格指数 d＝2.029 96；而 53 号的（100）晶面指数 d＝2.032 47，54 号则为 d＝2.035 08，这与 55 号试样相比，二者（100）晶面指数 d 值均增大；这表明 α-Fe 基体固溶了较多含量的 Cr 和 V 元素，从而基体具有较好的耐腐蚀性。另外，53 号、54 号的 XRD 图谱上未见 γ-Fe 的衍射峰，这说明加入一定量的钒，可明显降低基体组织的碳含量。由 Fe-Cr-V 堆焊合金的表面形貌图 3 可知，碳化物主要分布于晶界，少量以点状或者块状形式在晶内析出，晶界碳化物主要是 $(Cr,Fe)_{23}C_6$，呈条状或者断续网状。由于晶界析出高铬碳化物，

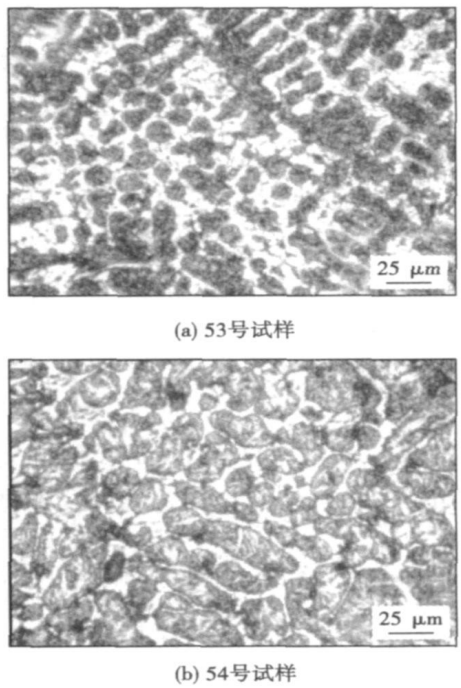

图 1 Fe-Cr-V 堆焊合金的金相组织

Fig. 1 Microstructure of Fe-Cr-V hardfacing alloy

而基体内铬原子的扩散速度远比碳原子的小，这使得碳化物边缘形成“贫铬带”[1]，该区域被优先腐蚀，如晶界碳化物尺寸较小，则易脱落，点状碳化物更加

明显。

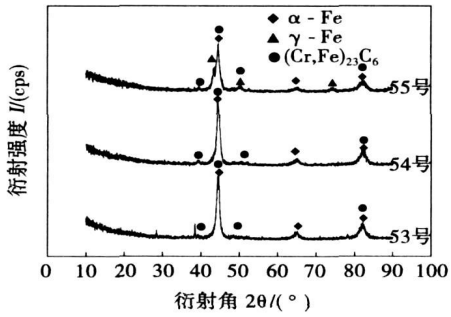

图 2　Fe-Cr-V 堆焊合金的 XRD 图谱

Fig. 2　XRD patterns of Fe-Cr-V hardfacing alloy

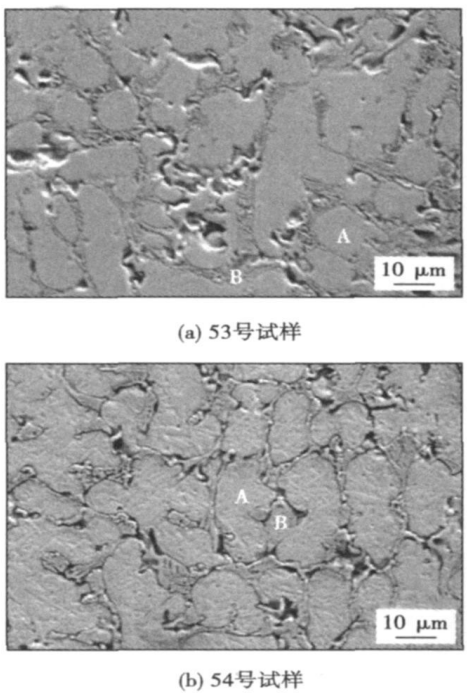

图 3　Fe-Cr-V 堆焊合金的表面形貌

Fig. 3　Surface morphology of Fe-Cr-V hardfacing alloy

用电子能谱仪 Oxford 7854 对 53 号、54 号试样的晶内与晶界微区(图 3 中的 A, B 点)进行成分探测，结果如下：图 3a 的 A 点(质量分数，%)为 Cr 9.6, V 1.29, B 点(质量分数，%)为 Cr 25.11, V 4.86；图 3b 的 A 点(质量分数，%)为 Cr 8.75, B 点(质量分数，%)为 Cr 31.39, V 7.15。结果显示，Cr, V 元素晶界含量显著高于晶内，并以碳化物形式出现于晶界；增加药芯焊丝中碳化钨等硬质相含量，V 元素晶界含量提高，而晶内含量减小，对铬含量分布影响结果也与之相同。这是由于晶内的 Cr、V 元素均主要以固溶形式存在于 α-Fe 基体，随着晶内硬质相或者析出相数量增多，α-Fe 基体晶格畸变加大，致使其可固溶元素量减少，另从 V 原子 (1.35Å)、Cr 原子(1.27Å)与 Fe 原子(1.27Å)半径差别可知，V 比 Cr 元素更易引起基体晶格的畸变，因而对 V 元素的分布影响相对更大。以上因素促使较多数量的碳化钒沿晶界析出，夹在 $(Cr,Fe)_{23}C_6$ 间，而碳化钒析出区域“贫碳”，形成铁素体，这促使晶间碳化物条状或者断续网状分布，晶界的抗裂性得以增强。

图 4 为钒含量及药芯焊丝中 B_4C 含量对 Fe-Cr-V 堆焊合金的硬度影响结果。由图 4a 可知，随着钒含量的增加，堆焊合金硬度提高；当钒含量增加到 2.0%时，其硬度值反而下降，这表明碳化钒析出数量越多，硬度愈高；但过量碳化钒析出，致使堆焊合金基体碳含量偏低，铁素体量增多，因而硬度下降。

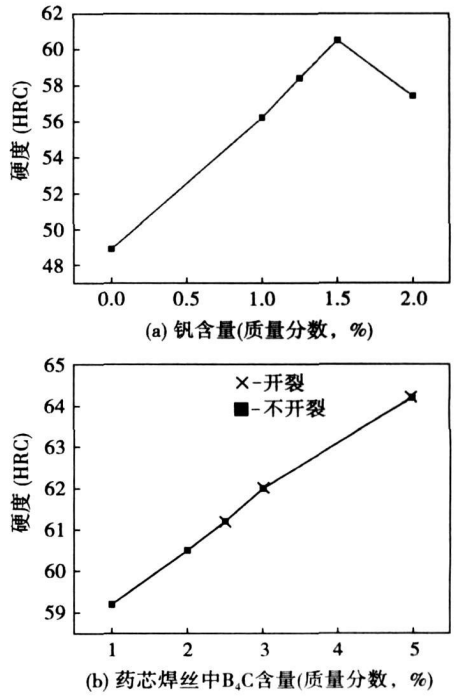

图 4　钒与 B_4C 含量对 Fe-Cr-V 堆焊合金硬度影响

Fig. 4　Effect of vanadium B_4C content on the hardness of Fe-Cr-V hardfacing alloy

硼化物具有高硬度和热稳定性，尤其以硼为主要合金元素的堆焊合金表现出优良的耐磨性[5]，但硼易与其它合金元素生成低熔点共晶或者硬脆相而产生裂纹。为了避免 B 和 Fe 等元素形成 FeB, Fe_2B 等脆性相，试验中硼以 B_4C 化合物的形式加入。由图 4b 可知，随着 B_4C 含量增加，堆焊合金硬度几乎呈线性上升，当药芯中加入量超过 2.5%(质量分数)时，堆焊合金开裂，加入量越大，硬度越高，但裂纹越多。以上结果说明，B_4C 可显著提高堆焊合金硬度，但也使其韧性下降，其加入量需控制在一定值以下。将 Fe-

Cr-V 堆焊合金药芯的 B_4C 置换为 NbC，其它组分保持不变。试验结果显示，堆焊合金极易产生冷裂纹，NbC 加入量越大，裂纹越多。NbC 的弥散分布虽可细化晶粒，提高基体的强度，增强 Fe-Cr-C 堆焊合金的耐磨性[6]，但也使基体中的 Cr 和 V 等元素的固溶量下降，晶界碳化物增多，因而合金韧性下降。

2.2 堆焊合金的耐磨性

表 2 为 Fe-Cr-V 堆焊合金的耐磨粒磨损试验结果，由此可知，堆焊合金的相对磨损系数 ε 只是实心焊丝 H25Cr3Mo2MnV 堆焊合金的 1.3 ~ 9.9%，具有良好的耐磨粒磨损性能。但耐磨性与硬度并不呈正比关系，而与堆焊合金的钒含量及药芯中的硬质相加入量相关，如将 46 号与 48 号、53 号与 54 号相比，它们仅药芯中 WC 加入量不同，但耐磨性相差大，这表明硬质相加入量对 Fe-Cr-V 堆焊合金的耐磨性影响显著。再从 46，52 和 53 号可以看出，堆焊合金的钒含量对其耐磨性的影响次之，这主要是因为晶内析出的碳化钒尺寸较小，在磨粒和水流的作用下易脱落，但碳化钒的弥散析出使基体强度得以改善。

从图 5 中 Fe-Cr-V 堆焊合金的表面磨损形貌来看，耐磨性试验后，表面残留凿槽或者犁沟条纹，其中 53 号试样的条纹较浅，有不少呈纵向分布，表面磨损较为均匀；而 54 号试样的条纹相对较深，纵向分布较少，可见二者磨损机制均是颗粒显微切削为主。材料的磨粒磨损率与其硬度成反比[7]，对金属硬

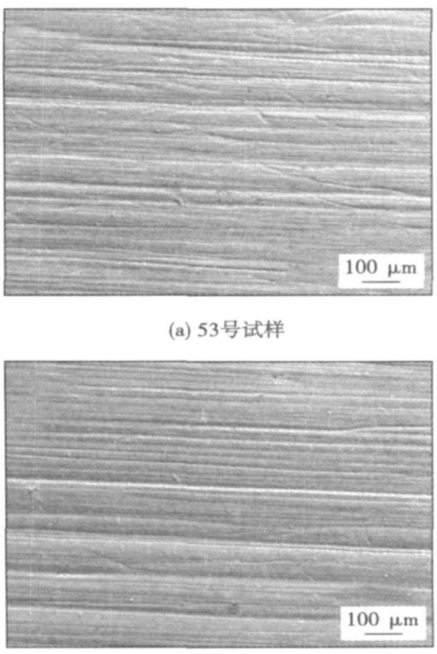

图 5 Fe-Cr-V 堆焊合金的耐磨粒磨损表面形貌

Fig. 5 Surface morphology of abrased Fe-Cr-V hardfacing alloy

度提高较多是碳化物质点，尺寸大的碳化物可以阻碍磨粒锲入堆焊合金表面，起到耐磨骨架作用。图 3 显示 54 号的晶界碳化物较粗大，53 号的碳化物颗粒较小，试验结果对应是 54 号的相对磨损系数 ε 是 53 号的 1.55 倍，这说明碳化物的尺寸大小直接影响堆焊合金的耐磨性。以上结果还表明，加入适量碳化钨，改善了碳化物的分布形态，从而提高堆焊合金的耐磨性。另外，磨损率还与基体的断裂韧性相关，碳化物过多，堆焊合金的断裂韧性下降，磨损率上升，因而，堆焊合金中不宜过多加入碳化物或碳化物形成组份。

3 结 论

（1）Fe-Cr-V 堆焊合金（质量分数（%）为：C 0.9 ~ 1.5，Cr 13 ~ 15，V 1.0 ~ 2.0，W 0.4 ~ 1.0，B 0.3 ~ 1.0 等）中，基体组织由铁素体＋马氏体组成，碳化物主要为 $(Cr, Fe)_{23}C_6$，该合金 Cr、V 元素晶界含量显著高于晶内，且碳化物形式存在于晶界。提高堆焊合金中 WC 量等硬质相数量，晶界的铬与钒含量增加，而晶内含量则减少。

（2）由于碳化钒沿晶析出，致使 Fe-Cr-V 堆焊合金的晶界碳化物 $(Cr, Fe)_{23}C_6$ 呈条状或者断续网状分布，起到耐磨骨架、阻碍磨粒锲入和减少磨粒切削量等作用，同时避免连续网状碳化物形态的强烈脆性，这使堆焊合金具有良好的耐磨性，同时降低了裂纹敏感性。

参考文献：

[1] 周振丰. 焊接冶金学（金属焊接性）[M]. 北京：机械工业出版社，1995.

[2] Kotecki D J. Hardfacing benefits maintenance and repair welding[J]. Welding Journal，1992，171(11)：51—53.

[3] 沈风刚，卢学军，许冷千，等. 热轧辊堆焊材料及工艺研究[J]. 机械工程材料，1998，20(4)：12—15.

[4] Kotecki D J，Ogborw J S. Abrasion resistance of iron-based hardfacing alloy[J]. Welding Journal，1995，74(8)：269s—278s.

[5] Yoo Jeong Wan，Lee Seong Hun，Yoon C S，*et al*. The effect of boron on the wear behavior of iron-based hardfacing alloys for nuclear power plants valves[J]. Journal of Nuclear Materials，2006，352：90—96.

[6] 王智慧，贺定勇. NbC 增强 Fe-Cr-C 耐磨堆焊合金组织与磨粒磨损性能[J]. 焊接学报，2007，28(2)：55—58.

[7] 李建明. 磨损金属学[M]. 北京：冶金工业出版社，1990.

作者简介：龚建勋，男，1973 年出生，博士，副教授。主要从事材料表面工程和功能薄膜方向的研究工作。发表论文 14 篇。

Email：gong309@tom.com

FCAW slag. The results show that the same weight CaO replacing MgO has an obvious improvement on the hydrogen dissolving capacity in slag. It's because the radius of the Ca^{2+} is bigger than the radius of the Mg^{2+} which has 12 match places, and easy to form the peroxide CaO, which can improve the oxygen content in slag. Some Al_2O_3 replacing MgO in FCAW slag will improve the hydrogen dissolving capacity in slag; the reason is the hydrogen has better solubility and diffusion coefficient in Al_2O_3.

Key words: welding; slag; diffusible hydrogen; dissolve hydrogen capacity

Modeling method for pulsed GTAW welding process based on variable precision rough set LI Wenhang[1], CHEN Shanben[2], WANG Jiayou[1], YANG Feng[1] (1. Institute of Welding Engineering, Jiangsu University of Science and Technology, Zhenjiang 212003, China; 2. Institute of Welding Engineering, Shanghai Jiaotong University, Shanghai 200030, China). p57—59, 63

Abstract: Considering the characters of welding process, a VPRS (variable precision rough set) modeling method is proposed for pulsed GTAW welding process. The VPRS model that can predict the backside width of welding pool is obtained. The main procedure of the modeling method and the key problems are expatiated. The result shows that the precise and complexity of the model is acceptable.

Key words: welding automation; modeling; variable precision rough set; GTAW

Calculation and discussion of welding plastic strain FANG Hongyuan, ZHANG Xueqiu, YANG Jianguo, LIU Xuesong (State Key Laboratory of Advanced Welding Production Technology, Harbin Institute of Technology, Harbin 150001, China). p60—63

Abstract: Numerical simulation method is employed to discuss welding longitudinal plastic strain distribution. Residual compressive plastic strain presents in the weld from traditional views, but the new viewpoint supports that the tensile plastic strain presents in the weld. Based on the two different viewpoints, the welding longitudinal plastic strain distribution is analysed with and without the fusion phenomenon according to the calculation results. The simulated results show that there exists little different in the two situations, and compressive plastic strain in the heating process is larger than tensile plastic strain in the cooling process. When a fusion phenomenon is considered, the heat affected zone still keeps the compressive plastic strain all the time, and only the plastic strain value in the cooling process is smaller than the one in the heating process.

Key words: residual stress; compressive strain; numerical simulation; temperature field; fusion phenomenon

Wear resistance of TiB_2-316L stainless steel matrix composite coatings deposited by atmospheric plasma spraying CHENG Hanchi, LI Zhuoxin, AN Shuchun, WU Yongzhi, LI Hong, SHI Yaowu (College of Material Science and Engineering, Beijing University of Technology, Beijing 100022, China). p64—68, 80

Abstract: TiB_2-316L stainless steel matrix composite powders contained 10mass% and 40mass% TiB_2 were prepared by high energy ball milling and spray-drying processes respectively. Atmospheric plasma spraying deposited corresponding coatings and 316 L stainless steel coating. High velocity block-on-ring wear tester was used to test wear resistance of as-sprayed coatings. X-ray diffraction analyzed the constitution of as-sprayed coatings. Scanning electron microscope was employed to character as-sprayed coatings, feedstocks and the worn surface morphology. Results show that wear resistance of as-sprayed TiB_2-316L stainless steel matrix composite coatings is prior to 316L stainless steel coating. TiB_2 particles act as reinforcement component in the coating and oxides from tribo-oxidation of TiB_2 in the tribo contact, which possessed self-lubricating function, can reduce mass loss of the coatings during sliding wear.

Key words: titanium-diboride; 316L stainless steel; ball-milling; spray-drying; atmospheric plasma spray

Discussion on principle of welding stress and distortion (2) WANG Zhechang (Institute of Metal Research, Chinese Academy of Sciences, Shenyang 110016, China). p69—72

Abstract: Formation and relief mechanism of welding residual stress were addressed. Compressive plastic strain dose not play a role in the formation of welding residual stress. The residual stress is produced by the contraction of weld metal and its vicinity during the cooling process at the temperature below its "mechanical melting point". Residual stress elimination does not employ the tensile plastic strain to reduce, withdraw or compensate the compressive plastic strain, but to convert the residual elastic strain to a plastic one. The elimination of the inherent strain is not a prerequisite to eliminate welding residual stress. Partly removed or completely held inherent residual strains can also completely eliminated the residual stress. A new method is proposed to perform heating treatment following the welding torch to control stress-strain precisely, to realize the stress free welding or stress-free and non-distortion welding or even proper compressive stress and non-distortion welding or large compressive stress and minor distortion welding. The result is also compared with the traditional processing method and finite element analysis.

Key words: welding stress-strain; compressive plastic strain; inherent strain; non-stress welding; non-stress-deformation welding

Fe-Cr-V wear resistant hardfacing alloy GONG Jianxun[1], XIAO Yifeng[1], ZHANG Qinghui[1], Ma Mo[2] (1. School of Mechanical Engineering, Xiangtan University, Xiangtan 411105, China; 2. Faculty of Material and Photoelectronic Physics, Xiangtan University, Xiangtan 411105, China). p73—76

Abstract: The Fe-Cr-V hardfacing alloy containing 0.9%—1.5%C, 13%—15%Cr and 1.0%—2.0%V was prepared for flux cored wire of submerged arc welding. The microstructure of hardfacing alloy was researched by means of optical microscopy, scanning electron microscopy, X-ray diffraction, etc. The effect of

vanadium content and B_4C in flux core on the properties of surfacing alloy was also studied. The microstructures of hardfacing alloy consist of ferrite, martensite and carbide such as $(Cr, Fe)_{23}C_6$. The micro-analysis with electron spectrometer show that the content of chromium and vanadium in grain boundary is richer than those in transgranular and the gap becomes bigger as WC content in flux core increases. The carbides distributing along grain boundary such as $(Cr, Fe)_{23}C_6$ appear strip or discontinuous network form, which caused by the precipitation of vanadium carbide. It plays a role as the skeleton to prevent cutting wear of abrasive particles and refrains from the strong brittleness of network carbide. Comparing to the deposited alloy of H25Cr3Mo2MnV solid wire, the abrasion resistance of Fe-Cr-V alloy was more deliberately excellent.

Key words: wear resistance; hardfacing; flux-cored wire; ferrite; carbide

Development of multi-funtions welding heat simulating software FENG Yingying[1], LUO Zongan[1], ZHANG Dianhua[1], SU Hailong[1], WANG Lijun[2] (1. State Key Laboratory of Rolling & Automation, Northeastern University, Shenyang 110004, China; 2. Science and Technology Stock Corporation of Angang, Anshan 114001, China). p77—80

Abstract: The software for welding heat simulating was developed successfully based on some classical mathematic models, measured data and programmed appropriately by LabVIEW8.2 and STEP7. The interface is simple to draw welding heat simulating curve with this software. Setting parameters of interval time for multi-pass welding heat simulating experiments can make the preheat temperature be consistent to the setting value. The software with good stability, reliability and conveniency has been applied to the series of domestic thermo-mechanical simulator, which consummates the simulator's functions.

Key words: welding heat simulating; mathematic model; multi-pass welding; interval time

Prediction of mechanical properties of welded joints based on RBF neural network ZHANG Yongzhi, DONG Junhui, ZHANG Yanfei (College of Materials Science and Engineering, Inner Mongolia University of Technology, Hohhot 010051, China). p81—84

Abstract: A RBF neural network model on the welding parameters and the mechanical properties of TC4 titanium alloy joints welded by TIG welding was established. The 27 sets of experimental data are used to train this model, and other 9 sets are used to simulation. The results show that the welding parameters including welding current, welding speed and argon gas flow rate as network input parameters can predict mechanical properties including tensile strength, bend strength and ductility. The efficiency and accuracy of the RBF network predictions have improved comparing with common standard BP neural network, which overcome the BP network's disadvantage of long time to train and plunge in part smallest easily.

Key words: RBF neural network; titanium alloy; prediction

Fatigue life prediction of SnAgCu soldered joints of FCBGA device ZHANG Liang[1], XUE Songbai[1], HAN Zongjie[1], LU Fangyan[1], YU Shenglin[1,2], LAI Zhongmin[1,3] (1. College of Materials Science and Technology, Nanjing University of Aeronautics and Astronautics, Nanjing 210016, China; 2. The 14th Research Institute, China Electronics Technology Group Corporation, Nanjing 210013, China; 3. Jiangsu University of Science and Technology, Zhenjiang 212003, China). p85—88

Abstract: Anand model was used to establish the constitutive equation of Sn3.0Ag0.5Cu solder, and the stress distribution of soldered joints was analyzed with and without underfill. The results indicate that the stress concentrates on the top surface of outermost soldered joint whether the underfill is here or not, and the stress decreases and distributes evenly on the top surface of soldered joint by using of underfill. The Modified Coffin-Mason equation by Engelmaier was utilized to predict the fatigue life of soldered joint; the fatigue life of soldered joint with underfill is longer than that without it. The effects of underfill properties were investigated. The results indicate that the CTE of underfill influences strongly the fatigue life of soldered joints, but the influence of Young's Modulus is little, which will provide a theory guide for practical applications.

Key words: constistutive equation; underfill; fatigue life

Interfacial reaction product and mechanical properties of the electron beam brazed Ni-based superalloy joints WANG Gang[1], ZHANG Binggang[1], HE Jingshan[1], FENG Jicai[1], JIANG Weiming[2], WU Yingjie[3] (1. National Key Laboratory of Advanced Welding Production Technology, Harbin Institute of Technology, Harbin 150001, China; 2. Jilin Petroleum Construction Metal Factory, Songyuan 138000, China; 3. Quality Control Department, Harbin Jiancheng Industry Company Limited, Harbin 150030, China). p89—92

Abstract: Ni-based superalloy K465 was brazed with BNi-p27 filler metal by vacuum electron beam brazing, and the effects of primary processing parameters on shear strength of joints were investigated. Microstructure of the brazed joints with BNi-p27 filler metal is studied by scanning electron microscopy (SEM), energy disperse spectrum (EDS) and X-ray diffraction (XRD). The results show that the structure of brazing seam consists of a large amount of γ solid solution, $(\gamma'+\gamma)$, rich W in Ni_3B and CrB, and a small quantity of NbC. With the beam current and heating time increasing, the tendency of shear strength of the joints firstly increased, and then decreased. The excellent shear strength of the joints is 436 MPa when the beam current of welding is 2.6 mA, heating time is 560s and focused current is 1 800 mA.

Key words: electron beam; brazing; interfacial reaction product; shear strength

Finite element analysis on influencing factors of soldered column